ADVANCED ENGINEERING MATERIALS

DOI: 10.1002/adem.200900061

Designing Ultrahigh Strength Steels with Good Ductility by Combining Transformation Induced Plasticity and Martensite Aging

By *Dierk Raabe,* Dirk Ponge, Olga Dmitrieva* and *Benedikt Sander*

Steels with a high ultimate tensile strength (UTS) above 1 GPa and good ductility [total elongation (TE) of 15–20% in a tensile test] are of paramount relevance for lightweight engineering design strategies and corresponding CO_2 savings, Figure 1.[1,2]

In this work, we report about a novel design approach for precipitation hardened ductile high strength martensitic and austenitic-martensitic steels (up to 1.5 GPa strength). The alloys are characterized by a low carbon content (0.01 wt% C), 9–15 wt% Mn to obtain different levels of austenite stability, and minor additions of Ni, Ti, and Mo (1–2 wt%). The latter are required for creating precipitates during aging heat treatment.

Hardening in these materials is realized by combining the TRIP effect with a maraging treatment [transformation-induced plasticity (TRIP); maraging: martensite aging through thermally stimulated precipitation of particles]. The TRIP mechanism is based on the deformation-stimulated athermal transformation of metastable austenite (face centered cubic Fe–Mn phase) into martensite (metastable body centered cubic or orthorhombic Fe–Mn phase) and the resulting matrix and martensite plasticity required to accommodate the transformation misfit.[3–11] The maraging treatment is based on hardening the heavily strained martensite through the formation of small intermetallic precipitates (of the order of several nanometers). These particles act as highly efficient obstacles against dislocation motion through the Orowan and Fine-Kelly mechanisms enhancing the strength of the material.[12–17]

While both types of alloys, i.e., TRIP steels[3–11] and maraging steels[12–17] have been well investigated, the combination of the two mechanisms in the form of a set of simple Fe–Mn alloys as suggested in this work, namely, the precipitation hardening of transformation-induced martensite by intermetallic nanoparticles, opens a novel and lean alloy path to the development of ultrahigh strength steels that has not been much explored in the past.[18,19] We refer to these alloys as maraging TRIP steels.

[*] *Prof. D. Raabe, Dr. D. Ponge, Dr. O. Dmitrieva, B. Sander*
Max-Planck-Institut für Eisenforschung, Max-Planck-Str. 1
40237 Düsseldorf, Germany
E-mail: d.raabe@mpie.de

Related steel design trends that are based on small-scaled second phase precipitates are also pursued by using oxide,[20–23] nitride,[24,25] or Cu nanosized particles.[26] Other pathways to the design of ultrahigh strength steels have been realized in ultra fine grained materials obtained by advanced thermomechanical processing[27–34] or by accumulative roll bonding.[35]

The joint maraging TRIP approach justifies a more detailed study since it opens up a new approach to increase the UTS of conventional steels at relatively lean alloying costs, i.e., without large quantities of expensive alloying elements, owing to the small volume fraction of precipitates required in maraging steels.[12–17] The negative side of such strategies lies often in the fact that an increase in tensile strength is typically accompanied by a corresponding drop in ductility, Figure 1.

In the current case, however, the opposite trend is found, i.e., we observe for two of the alloys under investigation (9 wt% Mn, 12 wt% Mn) the surprising simultaneous increase in both, strength and ductility upon aging. This most unexpected effect was not explained in the literature before.

The materials investigated combine in part different hardening mechanisms. The first one is the formation of mechanically induced martensite for the alloys with 0.01 wt% C and 12 wt% or respectively 15 wt% Mn which have retained austenite fractions between 15 and 50 vol%. This part of the approach follows, hence, the same hardening principles as conventional TRIP steels.[3–11] The second mechanism is the strain hardening of the ductile low carbon α'- and ε-martensite phases and of the remaining retained austenite in those cases where it is present. The third mechanism is the formation of nanosized particles in the as-quenched and also in the deformation-induced martensite during final aging. The latter heat treatment is, consequently, also referred to as martensite age hardening or maraging.[12–15]

The nanosized precipitates have a high dispersion owing to the good nucleation conditions in the heavily strained martensite matrix in which they form. Another aspect which might promote the formation of fine precipitates during cooling is the fact that the austenite, which contains the solute atoms required for the formation of precipitates in the martensite (Ni, Ti, Al, Mo), is stable until relatively low temperatures owing to the elevated Mn content. When during quenching the austenite becomes finally transformed into martensite the diffusion length of the atoms involved in precipitation is limited by the low temperature. While, in

COMMUNICATION

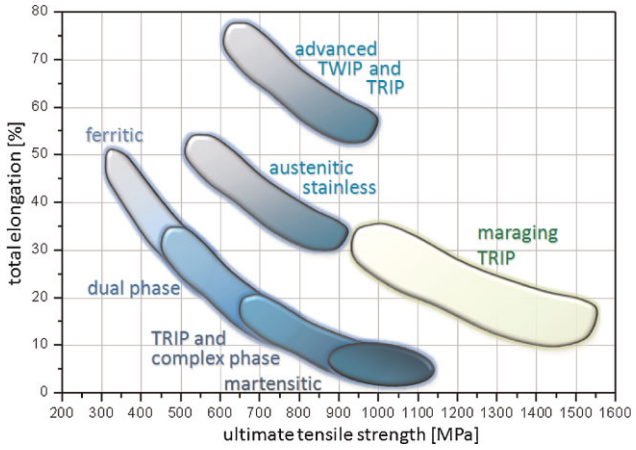

Fig. 1. Overview of the typical strength-ductility profiles of different types of steels. The strength is expressed in terms of the UTS measured during tensile testing and the ductility is expressed in terms of the total sample elongation. The data represent regimes such as published in the references given below. TRIP; TWIP; Complex phase: multiphase steels (e.g., austenitic-martensitic steels which may contain also bainite); maraging TRIP: new steel concept that includes hardening mechanisms based on TRIP and the formation of intermetallic nanoparticles in the martensite during aging. The approach leads to an unexpected simultaneous increase in both strength and TE (green area) enhancing the regime of formable ultrahigh strength steels by 0.5 GPa.

conventional Ni–Co maraging steels the nanosized precipitates are usually assumed to be ordered (intermetallic), the nature and composition of the precipitates encountered in the present alloys are not so clear yet.

Besides the optimization of yield strength (YS), UTS, and TE we also aim to design steels that are characterized by a homogeneous deformation behavior, hence the unexpected increase in TE upon aging is of high relevance. Most high strength steels [except for twinning induced plasticity (TWIP) steels] have a deficit with respect to the homogeneity of strain hardening since they reveal a drastic increase in strength at the beginning of deformation where it is not required but fail to provide sufficient strain hardening for the compensation of strain localization at later stages of deformation.

Here, we report about a 9 wt% Mn, a 12 wt% Mn, and a 15 wt% Mn alloy. All three materials have a very low carbon content and minor additions of Ni, Ti, Al and Mo to form nanoprecipitates. The main difference among the three alloys consists in the Mn content and hence, in the amount of retained austenite they contain (an increase in the Mn content lowers the equilibrium transformation temperature between ferrite and austenite). The results are compared to the mechanical properties of a conventional Ni–Co-based maraging steel.[12,13]

Materials, Experiments, and Characterization

Four alloys were investigated, namely, one standard 17 wt% Ni 11 wt%. Co maraging steel and the three maraging TRIP Fe–Mn steels (9 wt% Mn, 12 wt% Mn, 15 wt% Mn), Table 1.[12,13] The three Fe–Mn alloys have a low carbon content and minor additions of Ni, Ti, Al and Mo to form precipitates in the martensite.[36] The main difference among the three materials consists in their Mn content (~9, 12, and 15 wt%) and hence, in the volume fraction and stability of the retained austenite they contain after quenching.

The alloys were melted and cast to round billets of 1 kg each in a vacuum induction furnace. Annealing and swaging of the as-cast alloys was conducted to ensure homogenization of the microstructure and removal of segregation effects. After annealing at 1150 °C for 1 h swaging was conducted in eight passes between 1000 and 1150 °C. The billets were swaged from a diameter of 27.0–13.5 mm which corresponds to a logarithmic strain of 1.39. This was followed by air cooling to 800 °C and a water quench to room temperature. The rods were reheated to 1100 °C for 0.5 h, hot rolled in six passes to a total logarithmic strain of 1.9 into strips with a thickness of 4 mm and water quenched. These strips were cold rolled to a thickness of 1.5 mm corresponding to a logarithmic strain of 1. The subsequent solution heat treatment was performed at 1050 °C for 0.5 h followed by a final water quench. For heat treatments above 1000 °C argon gas atmosphere was used to prevent oxidation. Final aging heat treatments were conducted at different temperatures between 425 and 500 °C at times between 1 min and 48 h.

Flat tensile specimens were machined in the as quenched and in the solution treated state with a thickness of 1 mm, width of 4 mm and a gage length of 10 mm. A strain gage extensometer was used for precise determination of the strain. Tensile testing was conducted on a Zwick ZH 100 tensile testing machine at a constant cross head velocity corresponding to an initial strain rate of 8×10^{-1} s^{-1}.

Hardness testing according to EN ISO 6507-1 was conducted using a Zwick 3212 hardness tester to determine the Vickers hardness with a load of 49.05 N (HV5).

Characterization of the chemical and microstructural homogeneity of the cast, formed, and heat treated samples was conducted by using optical and scanning electron microscopy (SEM) in conjunction with EDX (energy dispersive X-ray spectrometry) and high resolution EBSD (electron back scatter diffraction). The SEM was a JEOL JSM-6500 F field emission SEM (FE-SEM) operated at 15 kV. The EBSD scans

Table 1. Alloy composition in weight % (wt%).

	C	Ni	Mo	Co	Ti	Si	Al	S	P	O	N	Mn	Fe
17 wt% Ni-11 wt% Co	0.024	17.20	3.89	11.4	1.55	0.078	0.176	0.003	<0.001	<0.0031	0.001	0.227	bal.
9 wt% Mn	0.0065	2.00	1.07	–	1.04	0.047	0.086	0.0023	<0.001	<0.002	0.0006	8.86	bal.
12 wt% Mn	0.0101	2.06	1.12	–	1.09	0.057	0.116	0.0101	<0.001	<0.002	0.0012	11.9	bal.
15 wt% Mn	0.0061	2.06	1.10	–	1.03	0.078	0.095	0.0046	<0.001	<0.002	0.0009	14.7	bal.

were carried out in areas of about $100 \times 270\,\mu m^2$ in cross sections in the middle of the samples at a step size of 100 nm. Additional high resolution EBSD maps were taken at 50 nm step size on $25 \times 25\,\mu m^2$ areas. Samples were ground using SiC paper (8 μm). Subsequently, the samples were mechanically polished using diamond suspensions of 3 and 1 μm. Final polishing was done using a SiO_2 suspension (0.1 μm). In order to study the possible influence of mechanical polishing on premature transformation of retained austenite (which is metastable against shear loads) samples were also prepared by electropolishing using 500 mL methanol, 500 mL 2-butoxyethanol, and 60 mL 70% perchloric acid for 20 s. Both preparation methods provided similar microstructure results.

Transmission electron microscopy (TEM) images were taken on the solution-treated, quenched plus finally age hardened sample with 12 wt% Mn in order to study the size and spatial distribution of the nanoparticles which are formed during aging. For TEM sample preparation the material was first thinned to a thickness below 100 μm by mechanical polishing. Standard 3 mm TEM disks were then punched and electropolished into TEM thin foils using a Struers Tenupol twin-jet electropolishing device. The electrolyte consisted of 5% perchloric acid ($HClO_4$) in 95% ethanol cooled to −30 °C. The thinned specimens were then investigated in the FE transmission electron microscope JEOL JEM 2200 FS operated at 200 kV. The analysis was carried out in scanning TEM mode (STEM) using a bright field (BF) detector.

The chemical composition of some of the nanoparticles observed in the material was studied at atomic scale resolution using atom probe tomography (APT) with a local electrode technique (IMAGO LEAP 3000× HR metrology device). This system provides an excellent mass resolution which is essential for the analysis of multi-component steels. The configuration includes a laser-based atom probe capability in addition to voltage pulsing. The measurements presented in this work were conducted in laser mode where the LEAP electrode applies a static field to the specimen while an ultra-fast laser pulse triggers the removal of the atoms. The use of the reflectron method used in the current configuration is important for an optimal time of flight (TOF) precision. Sample tip preparation for APT analysis was conducted using perchloric acid chemical etching.

Results

Figure 2 shows the mechanical data of the four alloys. Figure 3 presents the corresponding microstructure results

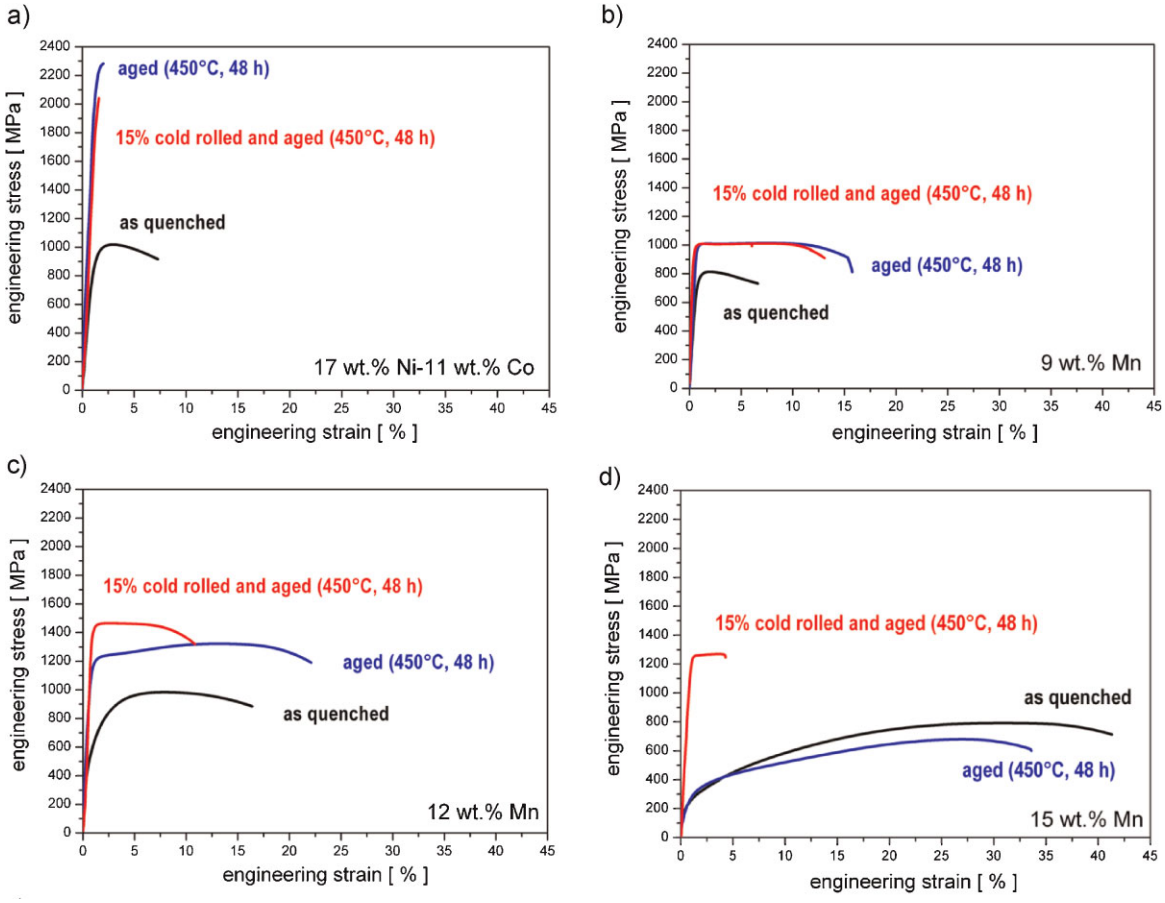

Fig. 2. Engineering stress–strain curves for the four steels, Table 1. (a) Standard 17 wt% Ni-11 wt% Co maraging steel; (b) Fe–Mn steel with 9 wt% Mn; (c) Fe–Mn steel with 12 wt% Mn; (d) Fe–Mn steel with 15 wt% Mn. All alloys have a very low carbon content and minor additions of Ni, Ti, and Mo to form precipitates. The main difference among the Fe–Mn alloys consists in their Mn content and hence, in the amount of retained austenite they contain. Three sets of data are shown, namely, in the as-quenched, age hardened, and 15% cold rolled plus age hardened state.

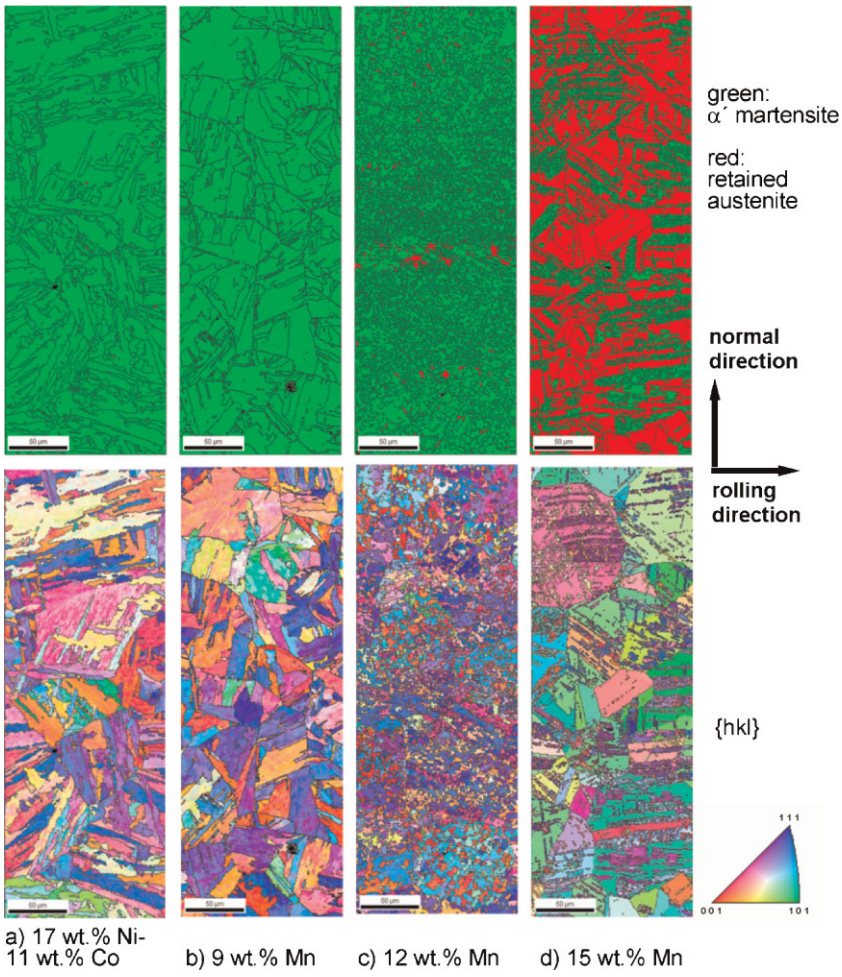

Fig. 3. Microstructure results for the four alloys obtained via EBSD analysis (100 nm step size). Top row: phase distribution of α′-martensite (green) and of retained austenite (red). Bottom row: microtexture in terms of the {hkl} Miller triple color coding and high angle grain boundaries (black, >15 °). (a) Conventional 17 wt% Ni-11 wt% Co maraging steel; (b) Fe–Mn steel with 9 wt% Mn; c) Fe–Mn steel with 12 wt% Mn; (d) Fe–Mn steel with 15 wt% Mn, Table 1.

(top row: phase distribution of α′-martensite and of retained austenite; bottom row: microtexture in terms of the {hkl} Miller triple and high angle grain boundaries). Figure 2a shows the engineering stress–strain curves of the conventional Ni–Co maraging steel in as-quenched, age hardened, and 15% cold rolled plus age hardened state.

The latter state was studied as the mechanical properties after pre-deformation prior to the tensile test may indicate the occurrence of a TRIP effect. The corresponding results obtained from phase and texture determination via EBSD are presented in Figure 3a, confirming that the Ni–Co maraging steel contains no or little retained austenite in the as-quenched state.

Figures 2b–d present the corresponding results for the three Mn-based steels (Fig. 2b, 9 wt% Mn; Fig. 2c, 12 wt% Mn; Fig. 2d, 15 wt% Mn).

The YS of the material with 9 wt% Mn is about 350 MPa, its UTS about 810 MPa, and the TE about 6% in the as-quenched state. The properties after aging heat treatment (48 h at 450 °C) are surprising. The UTS lies above 1 GPa (as expected) while the TE does not drop upon precipitation strengthening as observed for conventional Ni–Co-based maraging steels[12–16] but it increases from 6% to more than 15%. This means that precipitation hardening in this martensitic alloy simultaneously increases both strength and ductility. 15% pre-deformation (by cold rolling) of the same sample prior to aging yields similar properties as without pre-deformation. This results indicates that no retained martensite is involved. This is confirmed by the EBSD maps. The EBSD analysis for the 9 wt% Mn alloy (Fig. 3b) reveals coarse α′-martensite lamellae with longitudinal dimensions of up to 100 μm, but no retained austenite appears in the solution annealed and quenched state. This means that it is not an age hardenable TRIP steel (referred here to as maraging TRIP steel) but a Mn-based maraging steel.[18,19]

Similar observations are made for the microstructure of the 12 wt% Mn alloy, Figures 2c and 3c. This sample also consists of an α′-martensite matrix but it contains up to 15 vol% retained austenite and some ε-martensite. Hence, this material represents an age hardenable TRIP steel as it can undergo hardening both, via mechanically induced martensite formation and also through precipitation hardening of the as-quenched and of the mechanically induced martensite. The EBSD map for the 12 wt% Mn alloy shows a considerably finer α′-martensite microstructure than that observed in the 9 wt% Mn sample, Figures 3b and c. Dilatometry (measurement of thermal expansion) and ferromagnetic data suggest in part a higher austenite fraction of up to 20 vol%. The differences between dilatometry, ferromagnetic characterization, and EBSD analysis can be attributed to the limited statistics provided by EBSD. Also EBSD yields surface information only. The size of the retained austenite islands lies between 1 and 20 μm. The ε-martensite lamellae are below 2 μm and occupy an overall fraction of about 1–2 vol%.

The 12 wt% Mn alloy has a YS of about 325 MPa, UTS of nearly 1 GPa, and TE of about 16% in the as-quenched state, Figure 2c. After aging (450 °C for 48 h) the UTS increases to more than 1.3 GPa and the TE to 21%. 15% cold rolling prior to aging leads to a strong increase in strength (nearly 1.5 GPa UTS) but also to a drop in TE (about 10%).

Regarding the ductility it is most remarkable that both steels (9 wt% Mn and 12 wt% Mn) show, irrespective of their retained austenite content, the surprising feature of a simultaneous increase in both, UTS and TE upon aging. While the UTS increases by 25–30% the TE increases by more than 150% (from 6 to 15%) for the 9 wt% Mn sample and by

ADVANCED ENGINEERING MATERIALS

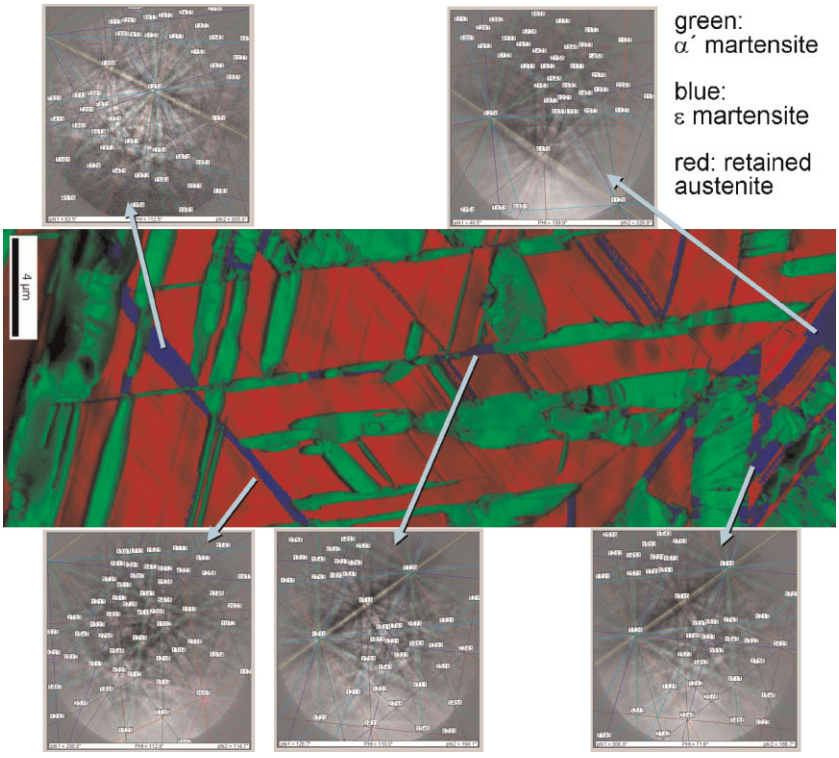

Fig. 4. High resolution EBSD analysis of the 15 wt% Mn steel showing details of the differentiation between retained austenite (red), α′-martensite (green), ε-martensite (blue) (50 nm step size).

31% (from 16 to 21%) for the 12 wt% Mn alloy. This increase in both properties represents a very unusual feature of these ultrahigh strength materials.

Figure 2d shows the engineering stress–strain curves for the 15 wt% Mn sample steel in as-quenched, age hardened, and 15% cold rolled plus age hardened state. The corresponding phase and texture maps are given in Figure 3d. The alloy contains a high volume fraction of retained austenite in the as-quenched state. The high resolution EBSD analysis presented in Figure 4 shows that in addition to α′-martensite the sample also contains some ε-martensite (marked in blue).[37]

The as-quenched 15 wt% Mn alloy has a YS of about 160 MPa, a UTS of about 800 MPa, and a TE of about 40%, Figure 2d. After aging (450 °C for 48 h) the UTS drops to about 700 MPa and the TE to 32%. 15% cold rolling prior to aging leads to a strong increase in strength (above 1.2 GPa UTS) but also to a drop in TE (about 3%).

This means that the steel with the most stable austenite and highest Mn content (15 wt%) does not reveal the same unusual feature of an increase in ductility upon aging heat treatment as the two steels with smaller Mn content (9 and 12 wt%).

The BF-STEM micrographs that were taken exemplarily on the age hardened maraging TRIP steel (12 wt% Mn) show that the nanoscaled precipitates reveal a narrow size distribution with an average diameter of 6–8 nm, Figures 5a and b. Figure 5b also reveals some of the retained austenite which is free of precipitates.

Local EDX analysis conducted in convergent beam mode show an increased content in Ni, Ti, and Al in these particles when compared to the surrounding matrix.[13,14,38] The area density of the nanoparticles was about 300 μm^{-2}. The corresponding volume density is estimated as $5 \times 10^3\ \mu m^{-3}$ (about 2–3 vol%), Figure 5. Slightly elongated nanoparticles were observed at the interfaces between the martensite lamellae.

In addition to the EDX-TEM analysis we also conducted APT measurements on the alloy with 9 wt% Mn. Figure 6 reveals a somewhat more complex composition of the precipitates. The APT maps show the joint occurrence of Ni, Al, and Ti in some of the clusters and also some isolated arrays where either Ni or Ti coincide with higher concentrations of Al. A more detailed atomic scale analysis inside some of these particles revealed a composition including not only Ni, Al, and Ti but also Fe and Mn enrichment. These observations indicate that the particles encountered do as a rule not assume a simple binary and ternary composition but seem to be more complex. In some case even the formation of tiny austenitic clusters or zones similar to the FeMn θ phase is conceivable.

Discussion

The stress–strain data for the different specimens show in principal two types of behavior before aging. The first two samples, i.e., the conventional highly alloyed 17 wt% Ni-11 wt% Co maraging steel and the maraging steel with 9 wt% Mn both reveal an α′-martensitic microstructure in the as-quenched state, Figure 3. This means that both materials do not contain metastable retained austenite, hence no TRIP effect occurs. Their mechanical performance, observed in tensile tests, Figures 2a and b, reflects this fact. Both materials reveal the same strength-elongation profile in the as-quenched and in the 15% pre-rolled state, i.e., no TRIP-related hardening was observed.

In contrast, the 12 wt% Mn and the 15 wt% Mn samples, Table 1, both show a pronounced increase in strength upon pre-deformation (plus subsequent aging), Figures 2 and 3. This observation is attributed to the mechanically-stimulated transformation of the retained austenite leading to a TRIP effect. Corresponding EBSD measurements show that the retained austenite present in both specimens in the as-quenched state is gradually transformed into martensite during deformation, Figure 7. The retained austenite is also present after heat treatment as the aging temperature (450 °C) was chosen below the temperature for re-transformation from martensite back into austenite. This point will be discussed in more detail below. Figure 7 shows high resolution EBSD data

COMMUNICATION

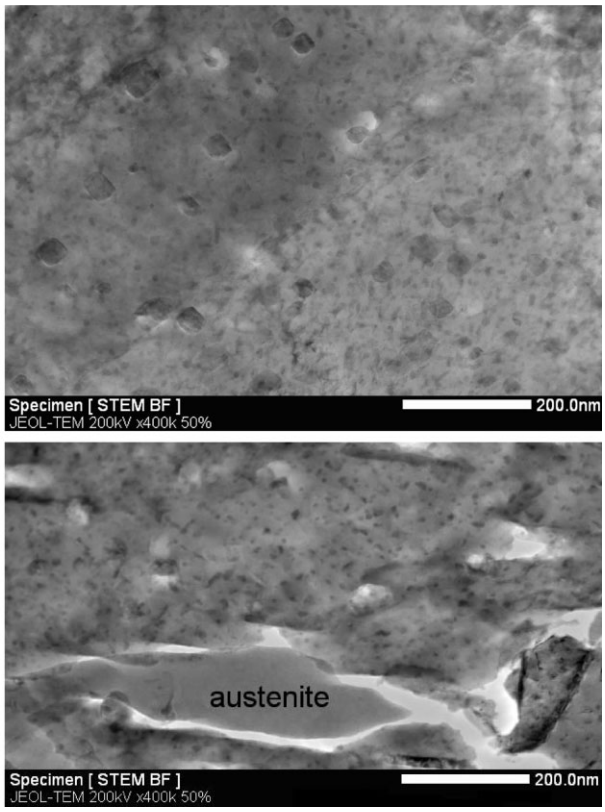

Fig. 5. TEM images of nanoparticles (and some larger particles) formed in the aged 12 wt% Mn alloy (450 °C, 48 h). The nanoparticles have an average diameter of 8–12 nm. Local EDX analysis shows an increased content in Ni, Ti, and Al in the particles relative to the matrix. (a) BF-STEM images of particles in two neighboring martensite lamellae. (b) BF-STEM images of particles in the martensite and particle-free austenite regions.

that were taken on the 12 wt% Mn sample in the as-quenched plus aged state, Figure 7a, and the same microstructure at uniform elongation in the deformed flat tensile specimen, Figure 7b.

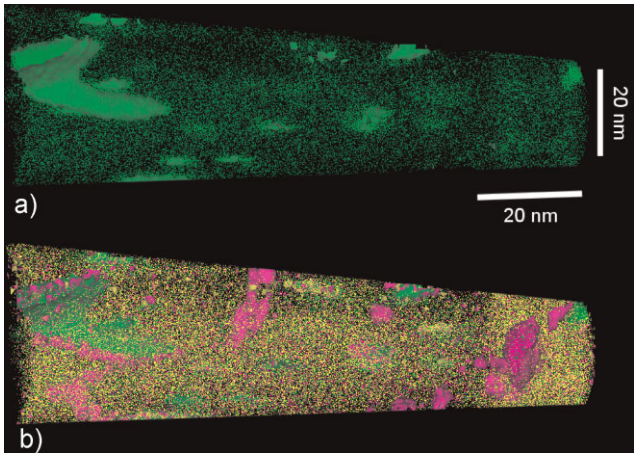

Fig. 6. ATP measurements (IMAGO LEAP 3000× HR) conducted on the maraging alloy with 9 wt% Mn. (a) Atomic distribution of the Ni content (green). The shaded zones indicate atomic Ni concentrations above 20 at.%. (b) Distribution of the Ni (green), Al (yellow), and Ti (magenta) clusters together with Al atoms (yellow). The shaded zones indicate an atomic Ni (green) concentration above 20 at.%, an atomic Al (yellow) concentration above 10 at.%, and an atomic Ti (magenta) concentration above 5 at.%. (a) (b)

The motivation for attributing the additional strain hardening capacity of the 12 and 15 wt% Mn alloys essentially to the TRIP effect becomes clear when comparing the data for the 15% pre-rolled specimens among the four samples, Figure 2. While, the samples with 12 and 15 wt% Mn contain retained austenite, Figure 5b, and, hence, show a strong increase in strength upon pre-deformation, the conventional Ni–Co maraging steel and the 9 wt% Mn samples both do not contain retained austenite and, therefore, do not reveal any change in strength when 15% cold rolled prior to tensile testing.

The second approach to classify the mechanical test result lies in the analysis of the unexpected ductilization upon aging observed for some of the specimens: Two alloys reveal a surprising increase both in strength and in the TE after aging, namely, the lean maraging steel with 9 wt% Mn (no or little retained austenite), Figures 2b and 3b and the maraging TRIP steel with 12 wt% Mn (containing retained austenite), Figures 2c, 3c, and 7.

For the 9 wt% Mn maraging steel we observe that the UTS increases by 25–30% to more than 1 GPa and the TE by more than 150% (from 6% TE to more than 15% TE) due to the aging heat treatment (450 °C for 48 h). For the 12 wt% Mn maraging TRIP alloy we observe after aging an increases in UTS to more than 1.3 GPa and of the TE from 16% to more than 21%. This increase in both mechanical properties (UTS, TE) represents a very unusual feature of these ultrahigh strength materials, Figure 1. All other strengthening methods explored so far in the field of ultrahigh strength steels lead to a decrease in the ductility rather than to its enhancement.[34]

The difference in the retained austenite content between the two alloys (9 and 12 wt% Mn) means that the unexpected ductilization effect seems not to coincide with the occurrence of the TRIP effect, as one of the materials does by practical standards not seem to contain retained austenite (9 wt% Mn).

The increase in strength upon aging heat treatment is attributed to precipitation hardening. The TEM and APT results, Figures 5 and 6, reveal that the steels contain nanosized particles such as also found in conventional maraging steels[12–17] and that the particle dispersion is very high, even after the long aging treatment (450 °C, 48 h) used in this study (shown here exemplarily for the 12 wt% Mn steel). The observation of a high maintained strength and high reluctance of the nanoscaled precipitates to coarsen was for conventional maraging steels reported before.[15] Using an Orowan line tension approximation for dislocation bow out between the nanoprecipitates with a particle diameter of about 10 nm and an average particle spacing of about 50 nm suggests a potential increase in the YS upon aging of about 400 MPa. This increase in the initial YS roughly matches the change in properties observed. The effect of the high dispersion on further strain hardening during deformation, in particular on deformation homogeneity, is even stronger than its effect on strength as will be discussed in more detail below using a Kocks–Mecking analysis.

Besides this strong effect of the nanoprecipitates formed during aging also the high retained dislocation content

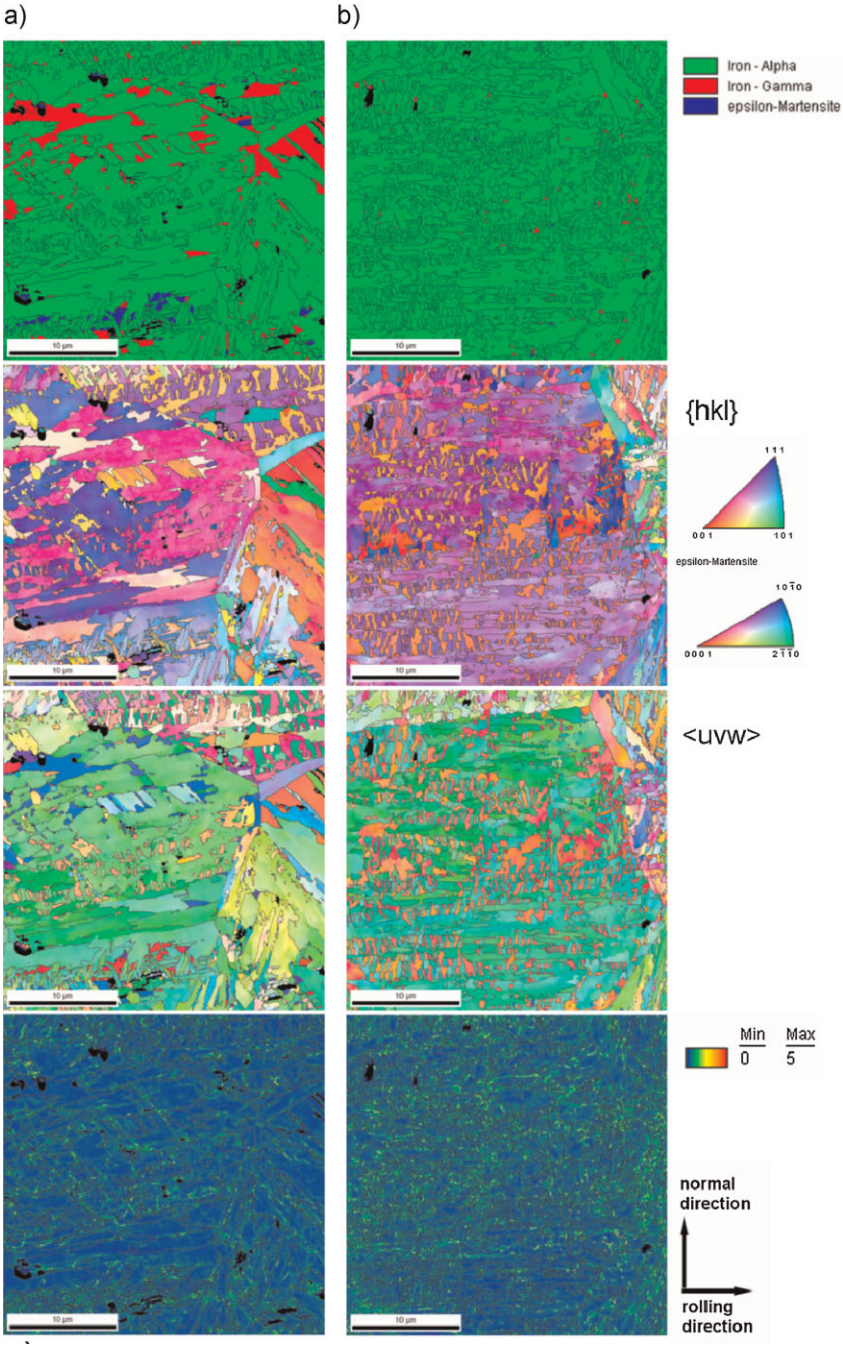

Fig. 7. High resolution EBSD maps taken on the 12 wt% Mn sample in the as-quenched plus aged state (a), and the same microstructure at uniform elongation in the deformed flat tensile specimen (b). The top row shows the phase content. The second row shows the texture in terms of the {hkl} Miller indices parallel to the normal direction. The third row shows the texture in terms of the <uvw> Miller indices parallel to the rolling direction. The bottom row shows the average local misorientation (50 nm step size).

observed in the martensite matrix is important for the high strength. The TEM data revealed that the dislocation density in the martensite is very high, about 10^{15}–10^{16} m^{-2}. It is noteworthy that the dense dislocation arrangement prevailed even after the aging heat treatment. The dislocation density could also play an important role for the nucleation of the precipitates and their very high dispersion, since we observed that many precipitates were located at dislocations.

It is also important for the plastic properties that the (nearly) carbon-free martensite matrix is rather ductile. Conventional carbon-based martensitic steels typically reveal very poor ductility, Figure 1.

However, irrespective of this plausible relationship between the nanoprecipitates and the increase in flow stress, a central point of our observations is the simultaneous strong increase in the TE after aging, Figures 2b and c. Two effects are conceivable to explain this phenomenon, namely, first, the kinetics associated with delayed austenitization and second, the kinetics of precipitation.

Regarding austenitization, it has been observed on conventional maraging steels that the heating rate and the holding times both influence the kinetics of re-transformation from martensite to austenite.[39] In other words, it is well conceivable that very long heat treatment times (450 °C, 48 h) entail delayed austenitization.

Dilatometry studies conducted at different heating rates confirm this phenomenon. Our data show the first deviation in length expansion from martensite upon re-heating at a temperature of about 550 °C for the 12 wt% Mn sample when using a quite rapid heating rate of 0.86 K s^{-1}. The same experiment conducted at a heating rate of 0.086 K s^{-1} revealed a lower transformation point from martensite into austenite around 500 °C. Thermodynamic predictions also suggest a transformation around 480 °C although some of the data underlying such simulations for Mn-containing Fe-based multi-component systems are not considered as very reliable.

In summary these considerations indicate that partial re-transformation into austenite might play a role for the ductilization at least for the specimen with 12 wt% Mn. On the other hand, the alloy with only 9 wt% Mn shows the same ductilization effect although partial re-transformation at 450 °C is thermodynamically not so likely for this alloy owing to it low austenite-stabilizing Mn content, Figure 2b.

A somewhat more plausible explanation for the ductilization effect can, hence, be seen in the Orowan hardening mechanism. Figure 8 shows the Kocks–Mecking analysis (strain hardening vs. true stress curve) for the two grades with 9 wt% Mn (no or little retained austenite) and 12 wt% Mn (at least 15 vol% retained austenite) together with the Considére line (strain hardening equals true stress). The data reveal in either case that the Orowan hardening effect is not active at the

COMMUNICATION

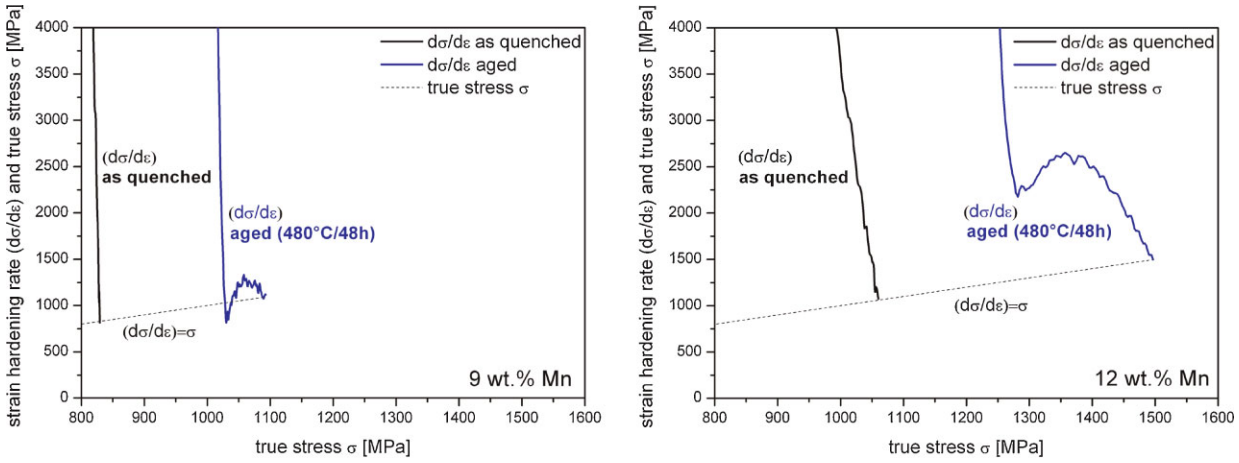

Fig. 8. Kocks–Mecking analysis (strain hardening vs. stress curve) of two alloys (9 wt% Mn, 12 wt% Mn) which reveals the background for the increase in TE upon aging heat treatment. Aging leads to a second hardening level at large stresses which does not appear in the as-quenched specimens. The intersections between the Considére lines (hardening equals true stress) and the hardening curves indicate the onset of mechanical instability.

beginning of the tensile test but occurs as a second hardening plateau at larger stresses, Figure 8. This plateau serves as a hardening reserve when the material starts to localize (Considére criterion).

The Kocks–Mecking curves for the as-quenched samples which were not heat treated and, hence, not aged, Figure 8, do not show a second hardening plateau. A corresponding analysis on the conventional Ni–Co-based maraging steel does not show this effect either before quenching. This confirms that the second hardening plateau can probably be interpreted in terms of Orowan hardening at least as the main mechanism. The reason that this effect does not occur at the beginning of straining is attributed to the fact that the inter-particle spacing is so small (~50 nm and below) that a higher stress level must be reached before Orowan loops can become active.

Conclusions

We presented a concept for the development of ultrahigh strength and at the same time ductile martensitic and austenitic-martensitic steels that is based on the precipitation of nanosized particles via aging heat treatment and, in some cases, on the TRIP effect. The approach, hence, combines the TRIP mechanism with a maraging treatment. The alloy systems presented are Fe–Mn steels with a low-carbon martensitic matrix and elements for the formation of nanoprecipitates (Ni, Ti, Al, Mo). Particularly the 12 wt% Mn maraging TRIP steel and the 9 wt% Mn maraging steel revealed a significant increase both in strength and TE after the aging heat treatment. The unexpected increase in TE was mainly attributed to the formation of nanoscaled particles leading to an Orowan hardening mechanism and to a second strain hardening plateau at intermediate strains.

Received: February 16, 2009
Final Version: April 9, 2009
Published online: June 22, 2009

[1] J. Inoue, S. Nambu, Y. Ishimoto, T. Koseki, *Scr. Mater.* **2008**, *59*, 1055.
[2] S. Nambu, M. Michiuchi, Y. Ishimoto, K. Asakura, J. Inoue, T. Koseki, *Scr. Mater.* **2008**, *59*, 1055.
[3] J. R. Patel, M. Cohen, *Acta Metall.* **1953**, *1*, 531.
[4] H. K. D. H. Bhadeshia, D. V. Edmonds, *Metall. Trans* **1979**, *10A*, 895.
[5] G. B. Olson, M. Cohen, in: *Mechanical Properties and Phase Transformations in Engineering Materials* (Eds: S. C. Antolovich, R. O. Ritchie, W. W. Gerberich), New Orleans Met. Soc. AIME, **1986**, pp. 367–390.
[6] M. Takahashi, H. K. D. H. Bhadeshia, *Mater. Trans JIM* **1991**, *32*, 689.
[7] P. J. Jacques, E. Girault, T. Catlin, N. Geerlofs, T. Kop, S. van der Zwaag, F. Delannay, *Mater. Sci. Eng, A* **1999**, *273*, 475.
[8] M. De Meyer, D. Vanderschueren, B. C. De Cooman, *ISIJ Int.* **1999**, *39*, 813.
[9] S. Traint, A. Pichler, K. Hauzenberger, P. Stiaszny, E. Werner, *Steel Res. Int.* **2002**, *73*, 259.
[10] P. J. Jacques, *Curr. Opin. Solid State Mater. Sci.* **2004**, *8*, 259.
[11] S. Zaefferer, J. Ohlert, W. Bleck, *Acta Mater.* **2004**, *52*, 2765.
[12] R. F. Decker, J. T. Eash, A. J. Goldman, *Trans. ASM* **1962**, *55*, 58.
[13] R. F. Decker, *Source Book on Maraging Steels*, ASM International, Metals Park, OH **1979**.
[14] W. Sha, A. Cerezo, G. D. W. Smith, *Metall. Trans.* **1993**, *24A*, 1251.
[15] V. K. Vasudervan, S. J. Kim, C. M. Wayman, *Metall. Trans.* **1990**, *21A*, 2655.
[16] C. Servant, N. Bouzid, *Acta Metall.* **1988**, *36*, 2771.
[17] R. Tewari, S. Majumder, I. S. Batra, G. K. Dey, S. Banerjee, *Acta Mater.* **2000**, *48*, 1187.
[18] A. J. Goldman, J. Manenc, *Trans. ASM* **1965**, *58*, 645.

[19] R. K. Ray, A. K. Seal, *Scr. Metall.* **1976**, *10*, 971.
[20] M. Alinger, G. Odette, D. Hoelzer, *Acta Mater.* **2009**, *57*, 392.
[21] G. R. Odette, M. J. Alinger, B. D. Wirth, *Ann. Rev. Mater. Res.* **2008**, *38*, 471.
[22] D. R. Lesuer, C. K. Syn, O. D. Sherby, *Mater. Trans.* **2006**, *47*, 1508.
[23] S. Yamashita, S. Ohtsuka, N. Akasaka, S. Ukai, S. Ohnuki, *Philos. Mag. Lett.* **2004**, *84*, 525.
[24] M. Taneike, F. Abe, K. Sawada, *Nature* **2003**, *424*, 294.
[25] E. Courtois, T. Epicier, C. Scott, *Micron* **2006**, *37*, 492.
[26] A. Machova, *Mater. Sci. Eng, A* **2001**, *319*, 574.
[27] L. Storojeva, D. Ponge, R. Kaspar, D. Raabe, *Acta Mater.* **2004**, *52*, 2209.
[28] R. Song, D. Ponge, R. Kaspar, D. Raabe, *Z. Metallk.* **2004**, *95*, 513.
[29] L. Storojeva, D. Ponge, D. Raabe, R. Kaspar, *Z. Metallk.* **2004**, *95*, 1108.
[30] R. Song, D. Ponge, D. Raabe, R. Kaspar, *Acta Mater.* **2004**, *53*, 845.
[31] R. Song, D. Ponge, D. Raabe, *Scr. Mater.* **2005**, *52*, 1075.
[32] R. Song, D. Ponge, D. Raabe, *ISIJ Int.* **2005**, *45*, 1721.
[33] R. Song, D. Ponge, D. Raabe, *Acta Mater.* **2005**, *53*, 4881.
[34] R. Song, D. Ponge, D. Raabe, J. G. Speer, D. K. Matlock, *Mater. Sci. Eng, A* **2006**, *441*, 1.
[35] N. Tsuji, Y. Saito, H. Utsunomiya, S. Tanigawa, *Scr. Mater.* **1999**, *40*, 795.
[36] D. Raabe, D. Ponge, O. Dmitrieva, B. Sander, *Scr. Mater.* **2009**, *60*, 1141.
[37] K. Verbeken, N. Van Caenegem, D. Raabe, *Micron* **2009**, *40*, 151.
[38] G. P. Miller, W. I. Mitchell, *J. Iron Steel Inst.* **1965**, *20*, 899.
[39] R. Kapoor, I. S. Batra, *Mater. Sci. Eng, A* **2004**, *371*, 324.

